Fixed bed reactors of non-spherical pellets
Importance of heterogeneities and inadequacy of azimuthal averaging

Mohammadzadeh Moghaddam, Elyas; Foumeny, E. A.; Stankiewicz, A. I.; Padding, J. T.

Contents lists available at ScienceDirect

Chemical Engineering Science: X

Fixed bed reactors of non-spherical pellets: Importance of heterogeneities and inadequacy of azimuthal averaging

E.M. Moghaddam, E.A. Foumeny, A.I. Stankiewicz, J.T. Padding *

Process & Energy Department, Delft University of Technology, the Netherlands

ABSTRACT

Despite the substantial simplicities inherent in pseudo-continuum models of fixed bed reactors, there is a continued interest in the use of such models for predicting fluid flow and transport scalars. In this paper, we aim to quantitatively address the inadequacy of 2D pseudo-continuum models for narrow-tube fixed beds. We show this by comparing with spatially resolved 3D results obtained by a robust and integrated numerical workflow, consisting of a sequential Rigid Body Dynamics and Computational Fluid Dynamics (RBD-CFD) approach. The RBD is founded on a physics-based hard-body packing algorithm, recently proposed by the authors (Moghaddam, E.M., Foumeny, E.A., Stankiewicz, A.I., Padding, J.T., 2018. A Rigid Body Dynamics Algorithm for Modelling Random Packing Structures of Non-Spherical and Non-Convex Pellets. Ind. Eng. Chem. Res. 57, 14988–15007), which offers a rigorous method to handle resting contacts between particles. The methodology is benchmarked for simulations of flow fields in all flow regimes, for $5 \leq Re_p \leq 3,000$, in random packings of spheres and cylinders with tube-to-pellet diameter ratios, N, between 2.29 and 6.1. The CFD results reveal a remarkable influence of local structure on the velocity distribution at the pellet scale, particularly in low-N packings, where the spatial heterogeneity of the structure is very strong along the bed axis. It is also demonstrated that azimuthal averaging of the 3D velocity field over the bed volume, which has been considered as an advancement over plug flow idealization in classical pseudo-continuum models, cannot reflect the role of vortex regions emerging in the wake of the pellets, and leads to underestimation of the local velocity values by more than 400% of the inlet velocity.

© 2019 The Author(s). Published by Elsevier Ltd. This is an open access article under the CC BY license (http://creativecommons.org/licenses/by/4.0/).

1. Introduction

Fixed bed unit operations have found extensive applications, particularly in reaction engineering, where they are used as the process workhorse in various chemical and process industries to handle highly exothermic and endothermic reactions. Such reactions require specific thermal management to prevent runaway reaction conditions. For this reason, narrow-to-moderate tubular fixed bed configurations are regularly employed, with tube-to-pellet diameter ratios, N, in the range of 2–10. The design of such reactors is usually performed on the basis of pseudo-homogenous models, wherein the essential role of topological non-uniformities and local flow maldistribution are neglected. This leads to failure of pseudo-homogeneous plug flow models in accurate prediction of the transport scalars at the pellet scale (Freiwald and Paterson, 1992; Papageorgiou and Froment, 1995; Vortmeyer and Haidegger, 1991). These inadequacies have led to numerous

experimental and analytical research efforts to incorporate the effects of bed structure, in particular the wall effect, into these models. Several investigators have employed non-invasive experimental techniques, e.g. McGreavy et al. (1986), Bey and Eigenberger (1997), Giese et al. (1998) and Krischke (2001) used Laser Doppler Velocimetry (LDV), and Mantle et al. (2001), Suekane et al. (2003), Ren et al. (2005), Baker et al. (2011) and Robbins et al. (2012) used Magnetic Resonance Imaging (MRI), Beguin et al. (2013) and Harshani et al. (2016) employed Particle Image Velocimetry (PIV), to investigate the flow field. Such methods are of limited coverage due to intrinsic restrictions connected to these non-invasive methods, as addressed by several researchers (Dijksman et al., 2012; Dixon et al., 2006; Harshani et al., 2016). A number of researchers has been inspired by the void fraction distribution over the bed radius, and tried to explain the radial inhomogeneities in the velocity field by flow channeling occurring near the wall region where the local porosity approaches unity. This observation has resulted in a simplified version of the radially dependent axial velocity profile, $v_z(r)$, from a modified momentum balance (Bey and Eigenberger, 2001, 1997) or a form of the

---

Nomenclature

d_p	Pellet diameter [m]		v_z	Azimuthally-averaged axial velocity [m/s]
d_{pv}	Diameter of a sphere of equal volume [m]		$v_z(r)$	Artificial velocity after Bey and Eigenberger (2001) [m/s]
d_{ps}	Diameter of a sphere of equal specific surface area [m]		Δp	Pressure drop [kg·m^{-1} s^{-2}]
d_t	Tube or bed diameter [m]		r	Radial coordinate [m]
I	Turbulence intensity [–]		z	Axial coordinate [m]
l	pellet length [m]			
N	Tube-to-pellet diameter ratio [–]			
N_{pv}	Tube-to-pellet diameter ratio based on d_{pv} [–]		*Greek letters*	
N_{ps}	Tube-to-pellet diameter ratio based on d_{ps} [–]		ε	Bulk porosity [–]
R_t	Bed radius [m]		$\varepsilon(r)$	Radial porosity profile [–]
Re_p	Reynolds number based on d_{pv}: $\rho_f u_s d_{pv}/\mu$ [–]		μ	Fluid dynamic viscosity [kg/(ms)]
u_s	Superficial velocity [m/s]		ρ_f	Fluid phase density [kg/m^3]
v_o	Inlet velocity [m/s]		Ψ	Pore-based friction factor [–]

Brinkman-Forcheimer-extended Darcy (BFD) equation (Giese et al., 1998), with pseudo-homogeneous models to account for the wall-effect in low-N fixed beds. Using such velocity-based pseudo-continuum models, e.g. the $\Lambda_r(r)$ model, several reactor studies have attained better agreement with experiments, e.g. (Giese et al., 1998; Bey and Eigenberger, 1997, 2001; Winterberg et al., 2000; Winterberg and Tsotsas, 2000a,b; Kwapinski et al., 2004). However, even these more sophisticated models are still based upon lumped (effective) properties, e.g. effective transport parameters. These lumped properties not only obscure the physical premise of the model, but also are very questionable for modeling low-N tubular fixed beds, where the cross-section contains only a few catalyst pellets, and thus azimuthal symmetry cannot be reasonably expected (Dixon et al., 2006; Freund et al., 2003, 2005; Nijemeisland and Dixon, 2004). In fact, a spatially resolved 3D simulation of the reactor system needs to be performed, so that the velocity, thermal and species concentration fields are thoroughly addressed (Dixon and Nijemeisland, 2001; Nijemeisland and Dixon, 2001). Over the last decade, advances in computer performance and computational techniques have allowed researchers to conduct comprehensive 3D simulations of flow fields and transport scalars within tubular fixed beds containing several hundred particles using Computational Fluid Dynamics (CFD) and Lattice Boltzmann methods (LBM), e.g. Augier et al. (2010), Boccardo et al. (2015), Coussirat et al. (2007), Dixon et al. (2012), Eppinger et al. (2011), Freund et al. (2005), Jafari et al. (2008), Magnico (2003), Nijemeisland and Dixon (2001), Pistocchini et al. (2016), Taskin et al. (2008), Wehinger et al. (2017a,b), Wehinger et al. (2015a,b), Yang et al. (2016). However, the majority of the prevailing efforts has concentrated on spherical packing structures, whilst application of catalyst pellets of non-spherical shape such as cylinders, Raschig rings, trilobe, quadrulobe, hollow extrudates, etc. is common in industry because of their potential to enhance transport processes (e.g. Raschig rings are used in ethylene epoxidation, and multi-hole shaped catalyst pellets are used in methane steam reforming units). The dominance of spherical packing studies can be attributed to the cumbersome and complicated strategies needed to generate a 3D surrogate model for packing structures of non-spherical pellets, which is an essential prerequisite for discrete-pellet CFD simulations. The orientational freedom of non-spherical particles makes the procedure of packing simulations very problematic, both in terms of modeling the collision phenomena and computational expense. Some researchers use the Discrete Element Method (DEM) to synthesize random packings of non-spherical pellets (Dong et al., 2017; Lu et al., 2015; Singhal et al., 2017a; Wehinger et al., 2015a,b, 2017a,b; Wu et al., 2017; Zhong et al., 2016). The most frequent approach in non-spherical DEM is the so-called glued-sphere method (Lu et al., 2015), in which the established framework of soft-sphere DEM is applied to model shaped particles and their collisions during the loading process (see Fig. 1).

Nevertheless, some research groups have employed the glued sphere approach in a CFD analysis of the local flow and transport properties in narrow-tube fixed beds of cylinder and Raschig ring pellets (Dong et al., 2017; Singhal et al., 2017a,b; Wehinger et al., 2015a,b). Wehinger et al. (2015a,b) have assessed the performance of the dry reforming of methane (DRM) process over three different pellets, including spheres, cylinders and Raschig rings, with N = 4.5, 3.6 and 3.6, respectively, using a sequential DEM and CFD method. The authors used a composite-sphere approach to generate random packings of solid cylinders, and used a post-treatment in CAD software to replace the solid cylinders with hollow cylinders, thus generating a Raschig ring packing structure. Even though interpenetration between Raschig rings during the packing process, due to the presence of an axial hole in the pellet's topology, is basically omitted using this strategy, the computed bulk porosity was in accordance with literature data. This may be caused in part by the inherently soft interactions used in DEM, allowing for a finite amount of overlap. The authors have discussed the behavior of the flow field and species transport inside the mentioned structures in the laminar flow regime. In another study, Wehinger et al. (2017a,b), dealt with the role of contact point treatment in CFD simulations of heat transfer in a tube stacked with cylindrical pellets. They used a multi-sphere model consisting of 100 DEM spheres as a surrogate model for a solid cylinder to synthesize a packing structure of cylinders with N = 4.17. Their analysis covers three flow conditions with particle Reynolds number Re_p = 191,
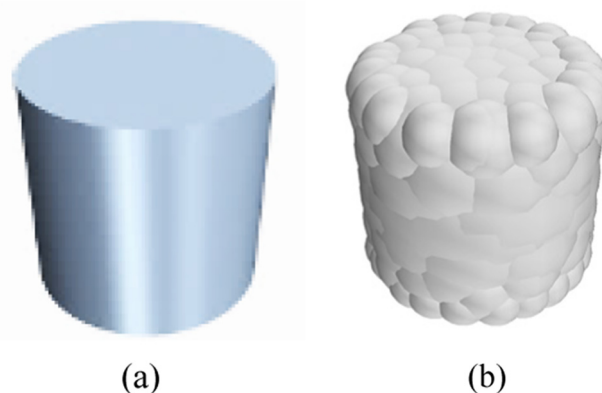
Fig. 1. (a) Actual CAD particle shape, (b) approximated by 100 DEM spheres; extracted from (Wehinger et al., 2017a).

382 and 763, corresponding to the experimental work of Bey and Eigenberger (1997). Dong et al. (2017) investigated the behavior of radial heat transfer in tubular fixed beds of glass spheres (N = 7) and steatite rings (N = 3.39) using a sequential DEM and CFD approach in the laminar flow regime, where Re_p was in the range of 60 to 100. The investigators pursued the same approach as Wehinger et al. (2015a,b) to generate a geometrical model for steatite rings, and validated their CFD results of heat transfer by comparing radial temperature profiles extracted from CFD results to their own experimental data. Singhal et al. (2017a,b) have also performed resolved-particle direct numerical simulation using a sequential glued-sphere DEM and CFD approach to investigate pressure drop and heat transfer in an extracted model of fixed beds of spheres and cylinders with different aspect ratios (2, 4 and 6) at $Re_p < 200$. The authors have presented some correlations for fluid-pellet film heat transfer Nusselt number.

Unfortunately, the approximation of non-spherical pellets by the composite-sphere method can lead to inaccurate contact force computations, particularly when collisions occur (Lu et al., 2015; Marigo and Stitt, 2015; Wachs et al., 2012). This has persuaded researchers to improve the multi-sphere DEM, e.g. Rakotonirina and Wachs (2018), Yan et al. (2015). Furthermore, alternative approaches to model collisional contact in non-spherical particles have recently been proposed and applied to different problems, addressing different issues for modelling non-spherical particles using DEM: Höhner et al. (2014) used a polyhedral approximation scheme, Ma and Zhao (2018) used a super-quadrics method, and Seelen et al. (2018) used a method based on the GJK algorithm. To the best of our knowledge, such modifications and alternative approaches have not been yet compiled and developed in an integrated methodology for implementing resolved-particle CFD modelling of fixed bed systems.

The application of Rigid Body Dynamics (RBD) in the field of chemical reaction engineering has been recently introduced by Boccardo et al. (2015). The authors have employed an open-source workflow based on Blender (which uses the Bullet Physics Library), which is a graphics and animation software released by the Blender Foundation, to generate random packings of spheres, cylinders and trilobes with N = 16.1, 27 and 23.3, respectively. The investigators then utilized the packing geometries for a CFD analysis of the flow field and pressure drop using OpenFOAM CFD code. Following this, Partopour and Dixon (2017) proposed an automated package, also based on the Bullet Physics Library to computationally generate and mesh resolved-particle packed beds of spheres, hollow cylinders and trilobes. The authors examined their workflow in studies of heat and reaction in fixed bed reactors. Overall, progress in discrete-pellet CFD modelling of fixed bed reactors is hampered by the complexities associated with the construction of realistic non-spherical packings. In the current contribution we will introduce and validate a robust workflow for implementing numerical experiments predicting the hydrodynamics in fixed beds containing non-spherical pellets. The workflow consists of a sequential Rigid Body Dynamics and Computational Fluid Dynamics (RBD-CFD) approach. The RBD is founded on a physics-based hard-body packing algorithm, recently proposed by the present authors (Moghaddam et al., 2018), in which a substantial improvement is offered for modelling the resting contacts compared to Blender software. A high-quality graded mesh is generated in the void space around the particle for CFD analysis of the hydrodynamic behavior in such a complicated unit operation. We will validate the results of this workflow against known experimental data, and will deal with the inadequacy of azimuthal averaging of the 3D velocity field over the bed volume in low-N packed columns of spheres and cylinders.

This paper is organized as follows: in Section 2 we summarize our workflow, in Section 3 we describe the setup of our simula-

tions, and in Section 4 we verify and validate our methodology, and show why 2D pseudo-continuum models are inadequate for low-N reactors. We end with our conclusions in Section 5.

2. Workflow

2.1. Step 1: Discrete pellet modeling of random packing structures

The first essential step in the simulation of flow through random packing structures is to generate a realistic 3D model of the packing topology. For this step, the physics-based Rigid Body Dynamics algorithm (see Moghaddam et al., 2018 for details and validation) is employed to synthesize random packings of spheres and solid cylinders. The RBD-based packing procedure can handle any non-spherical, even non-convex, pellet shapes. The essential features of RBD are (i) that each pellet is described by a triangular face mesh in a global coordinate system (see Fig. 2), (ii) that collisional contacts are handled as hard-body collisions, instead of the soft-particle approach used in DEM, and (iii) that resting contacts between multiple particles are modelled explicitly based on relative velocities, where the transition between moving and resting particles is controlled by a cut-off on the relative contact velocities. The former feature allows for simulation of pellets with sharp edges. The second feature avoids unphysically large overlap of particles caused by artificially lowered spring stiffnesses, frequently employed in DEM simulations to prevent unfeasibly small time steps in the treatment of particle collisions. The third feature avoids simplistic approaches to handle resting contact conditions, such as the artificial damping of linear and angular velocities adopted by graphical software like Blender. As illustrated in Fig. 2, the sharp edges of the cylindrical pellet are well-reproduced by the polygonal modeling used in the RBD-based packing algorithm. In contrast, the glued-sphere method leads to a poor approximation of the edges (see Fig. 1), which can result in imprecise prediction of contact forces, and accordingly erroneous packing structures.

The physical dimensions used to synthesize realistic random packings of spheres and cylinders are given in Table 1.

After the pellets have settled in the container, information about the simulated packings, in particular bulk porosity and radial porosity profiles, is generated using a post-processing mesh-based analysis, as elaborated in Moghaddam et al. (2018). Typical results of computer-generated packings are illustrated in Fig. 3.

2.2. Step 2: Contact point treatment

The second step in the workflow is to transfer the details of the packing structure, i.e. the position and orientation of each non-spherical pellet, to a mesh developer software. To this end, the face mesh data of each pellet is extracted and imported to Ansys Workbench 16.2 to produce a CAD model of the packing structure. One of the most important issues before meshing such a complicated topology is to deal with the contact points. Near contact points, the computational cells are in danger of becoming exceedingly skewed, meaning that some of their surfaces can be much larger than others, which can result in convergence problems in the turbulent flow regime. A detailed assessment of the prevailing alternative treatments for the contact point problem in fixed beds of spheres was performed by Dixon et al. (2013, 2012). Local treatment methods, such as the so-called bridge and cap methods, cannot be straightforwardly applied to non-spherical packings. An alternative is to apply the shrink-wrap method, which is a conventional approach to meshing ill-synthesized geometries such as structures containing interpenetrating parts, holes and gaps, to generate bridges at contact points of even non-spherical particles
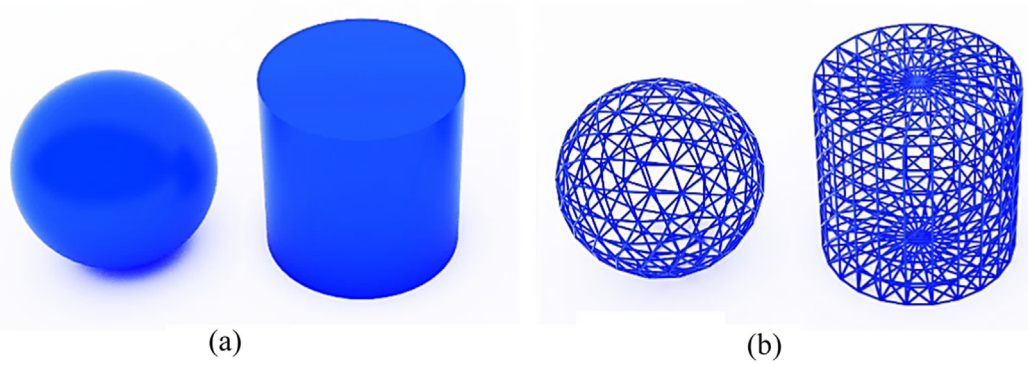
Fig. 2. 3D model of a sphere (d_p = 10 mm) and a cylinder (l = d_p = 10 mm). (a) The exact 3D model of pellets built in Ansys Workbench 16.2; (b) The model described by a face mesh for the RBD algorithm (Moghaddam et al., 2018).

Table 1
Specification of RBD-simulated packing structures (quantities are introduced in the nomenclature section).

| Pellet shape	Pellet size (mm)	Tube size (mm) H = 120 mm	N (d_t/d_p)	Particle count up to H = 100 mm
Sphere		31	3.1	73
	d_p = 10	41	4.1	131
		61	6.1	319
Cylinder	d_p = l = 10	22.9	2.29	48[*]
	d_{pv} = 11.45	35.5	3.55	63
	d_{ps} = 10	45.8	4.58	126

[*] This particle count is up to a height of H = 200 mm.
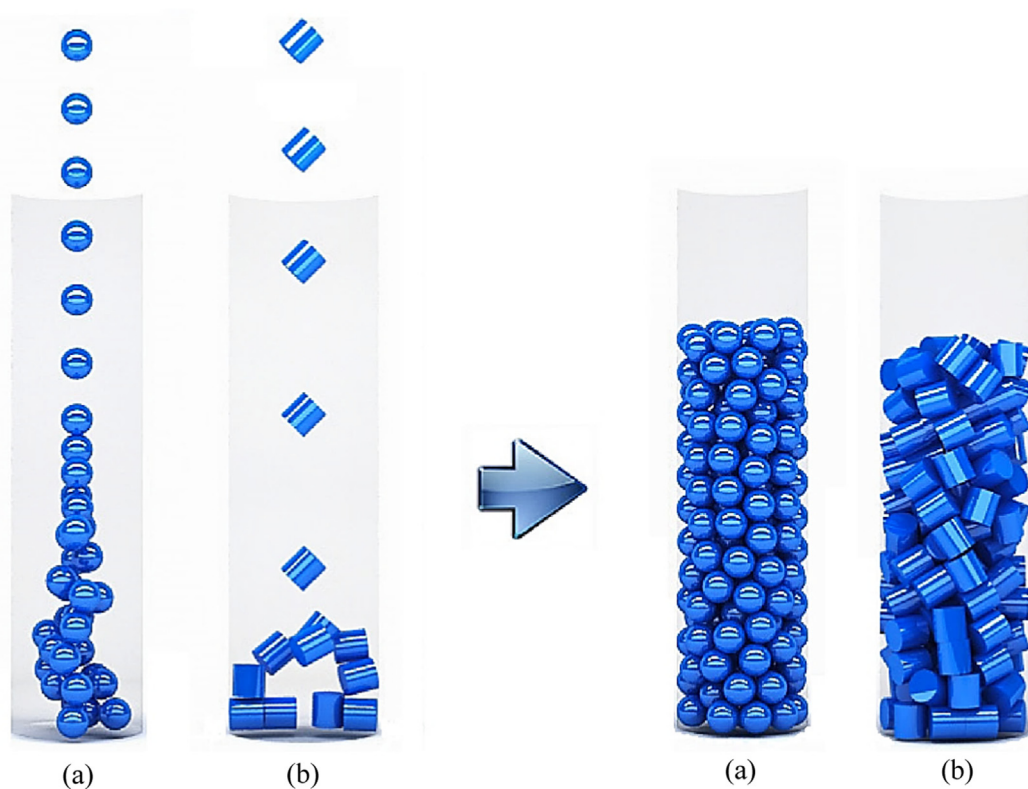
Fig. 3. Typical results of random packings simulated by the RBD-based packing algorithm; (a) spherical packing with N = 4.1, (b) cylindrical packing with N = 4.58.

(Partopour and Dixon, 2017). In this contribution, we applied the global gap approach because the quality of face meshes in the simulated structures is quite high. In this method, all pellets in the reproduced packing model are locally shrunk by 0.5% of their nom-

inal diameter around their respective centers of mass, resulting in an interstice at each contact region. Imposing such a small interstitial space can resolve the convergence problem by creating a computational mesh with appropriate skewness in such regions
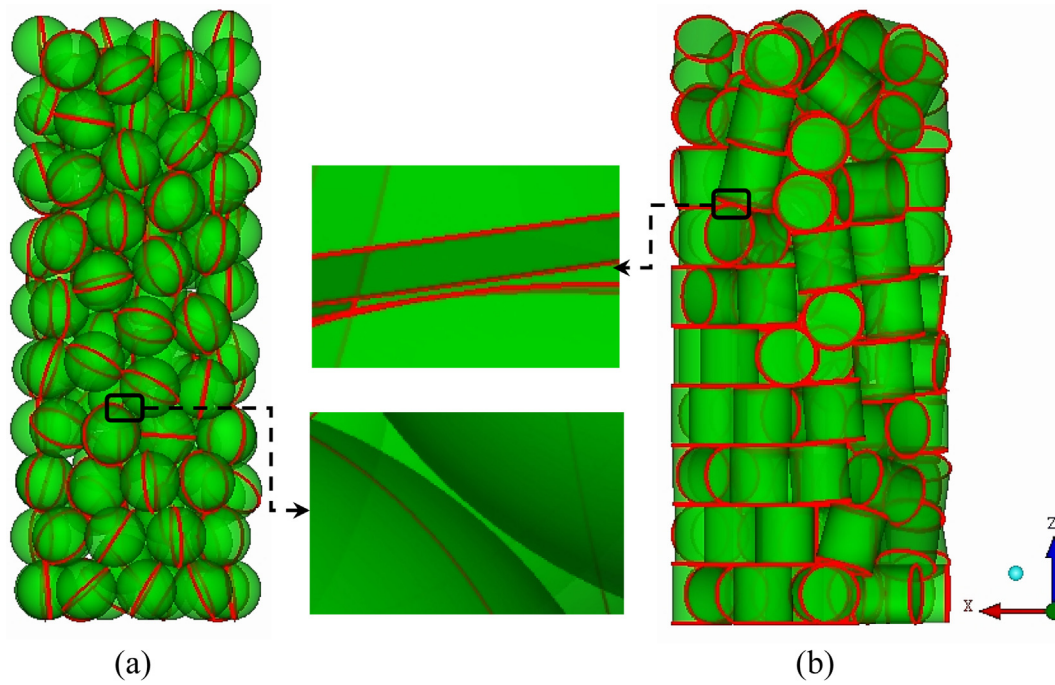
Fig. 4. Reconstructed models of the RBD-generated packings in Ansys Workbench 16.2 with a 0.005d$_p$ gap; (a) spherical packing with N = 4.1, (b) cylindrical packing with N = 4.58. Red lines indicate the sharp edges of the cylinders (and a random equator for the spheres). (For interpretation of the references to color in this figure legend, the reader is referred to the web version of this article.)
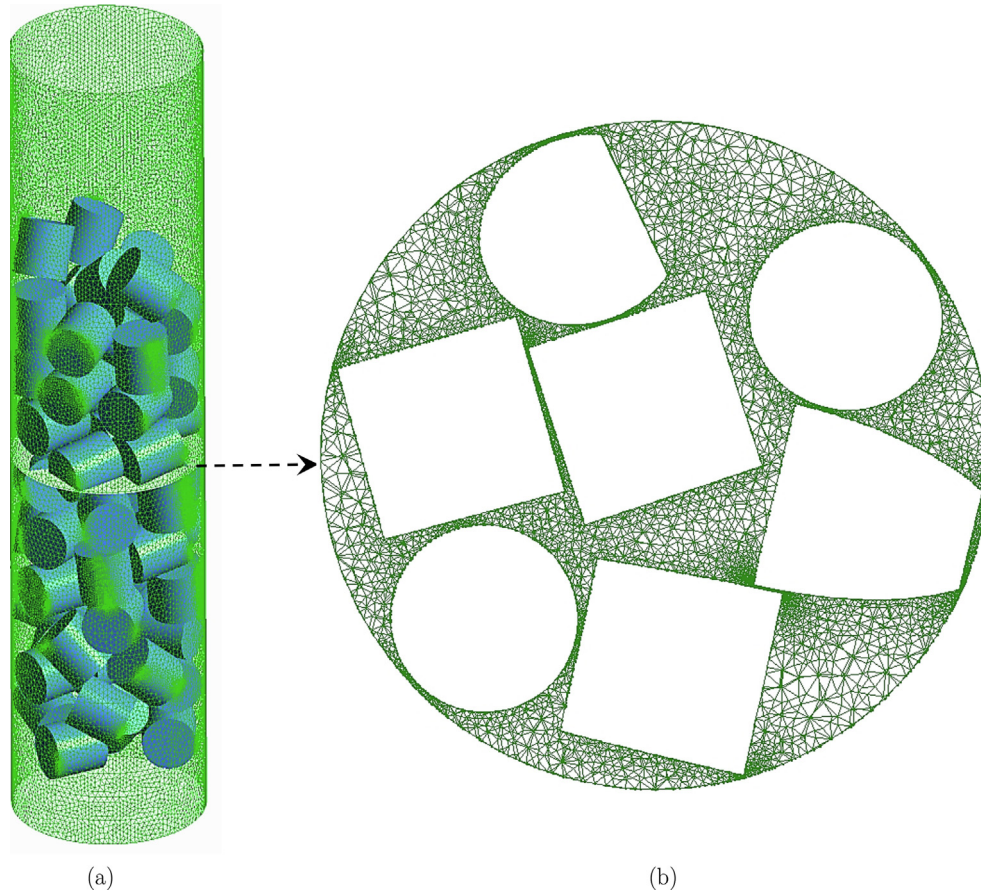
Fig. 5. Graded mesh topology in random packing of cylinders with N = 3.55 based on a medium mesh level (see Table 3); (a) face mesh on the tube wall, (b) a cut plane of the volume mesh at height z = 6d$_p$.

(see step 3). The shrinking factor should be kept sufficiently small to have a negligible effect on the bulk porosity of the packings, and to prevent jet formation in the gap regions at high Re_p conditions. Fig. 4 shows the reconstructed (CAD) models of spherical and cylindrical packings including contact point refinement.

2.3. Step 3: Meshing

The third step in the workflow deals with generating a high-quality mesh for CFD simulations. As always, there is a compromise between the face mesh quality, i.e. fine or coarse, and the accuracy and computational expense. In this work an advanced meshing approach, based on a combination of patch-independent and patch-conforming mesh methods, is implemented to generate a graded mesh topology for a random packing structure. This meshing approach is founded on a top-down meshing method to create an inflationary face mesh topology. This is controlled by an ad hoc Python-based script in Ansys Workbench. Following this, a bottom-up meshing method based on the Quick (Delaunay) tech-

nique is applied to create a graded volume mesh in the void spaces. Furthermore, to achieve a precise prediction of the velocity field in the near wall region, which depends on reliable prediction of wall-bounded turbulent flows, a number of prismatic layers were implemented on the solid surfaces, i.e. both tube wall and pellets, (Calis et al., 2001; Dixon et al., 2011; Romkes et al., 2003; Taskin et al., 2008). Our boundary-layer treatment for the flow simulations in the turbulent regime consisted of six layers of prisms with an initial height of 2.5×10^{-6} m, and a growth factor of 1.2, leading to a total prism depth of 2.48×10^{-5} m. This allows the laminar sublayer to be resolved for the highest inlet Re_p by obtaining the recommended dimensionless distance parameter, i.e. $y^+ \sim 1$ (y^+ is the dimensionless wall distance, which is used to describe wall-bounded turbulent flow). Fig. 5 shows how the proposed inflationary meshing scheme results in finer grids at the contact regions.

3. CFD setup

CFD simulations of fluid flow were performed for the random packing models addressed in Table 1 in the laminar, transitional and turbulent flow regimes, using the finite volume code ANSYS Fluent 16.2. The fluid phase was assumed to be isothermal and incompressible with the standard physical properties of air (ρ = 1.225 kg/m^3, μ = 1.7894 $\times$ 10^{-5} Pa.s). The air enters from the bottom of the packed column with a unidirectional and uniform velocity to provide a consistent basis for further comparison. The inlet air velocities were chosen in accordance to the desired particle Reynolds number Re_p (based on the volume-equivalent pellet diameters) ranging from 5 to 3000. These inlet flow conditions also cover the flow conditions used in the experimental work of Krischke (2001). To provide a consistent basis for comparison, the initial inlet turbulence intensity (for $Re_p \geq 200$) is computed based on the formula $I = 0.16\,Re^{-1/8}$. No-slip boundary conditions were applied to the column wall and pellet surfaces. For the bed outlet, a pressure-outlet boundary condition was defined. Furthermore, to minimize boundary effects at the column inlet and outlet, the bed entry and exit are extended by 1 and 6 particle diameters, respectively. A schematic overview of the flow model and boundary conditions is given in Fig. 6.

The governing equations for CFD simulations of hydrodynamics include the equations of conservation of total mass (continuity) and momentum for the laminar flow regime ($Re_p \leq 100$). For fully-turbulent flow, i.e., $Re_p \geq 600$, a Reynolds-Averaged Navier-Stokes (RANS) model was used, using the realizable $k-\varepsilon$ model with an Enhanced-Wall-Treatment (EWT) to model the turbulence. Compared to the standard $k-\varepsilon$ model, this model has an improved modeling of the turbulent energy dissipation rate (ε) and applies a variable C_μ instead of a constant value, offering a more sophisticated approach for simulation of flow fields with strong streamlines curvature, vortices and rotations, as typically found in random packing structures (Patankar, 1980). In the transitional flow regime, both the (laminar) Navier-Stokes equations and the realizable $k-\varepsilon$ model were examined.
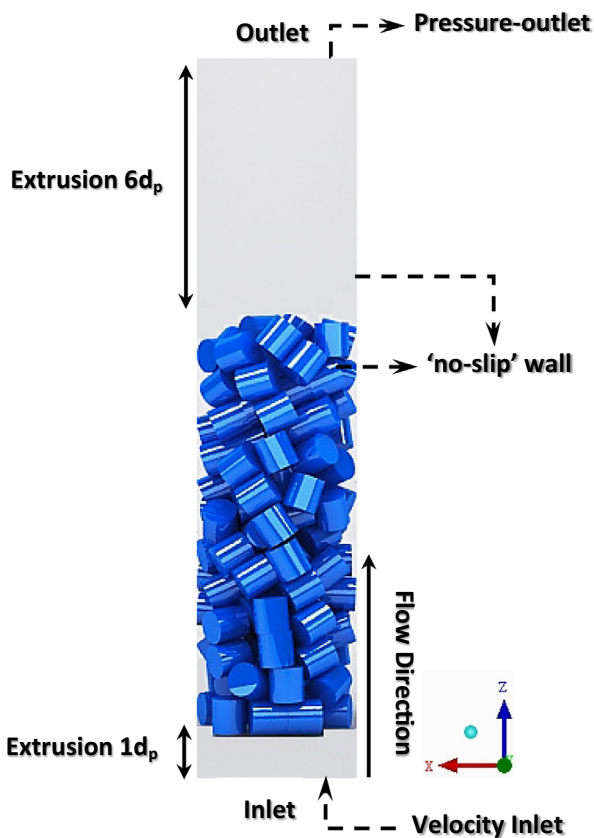

Fig. 6. Schematic overview of cylindrical packing model and boundary conditions used in the CFD simulations; N = 4.58.

Table 2
Bulk porosity results of RBD-simulated Structures.

Pelletshape	N(d_t/d_p)	Bulk porosity analysis (based on packing structure up to H = 120 mm)					Bulk porosity (after contraction)
		Simulated packings	Dixon, 1988	MRE (%)	Foumeny et al., 1991	MRE (%)	
Sphere	3.1	0.462	0.459	−0.65	0.463	0.22	0.470
	4.1	0.435	0.437	0.46	0.432	−0.69	0.443
	6.1	0.409	0.419	2.38	0.409	0.04	0.418
Cylinder	2.29	0.58	0.585	0.85	0.525	−10	0.583
	3.55	0.477	0.465	−2.60	0.414	−15.2	0.485
	4.58	0.386	0.429	9.97	0.377	−2.51	0.395

To solve the governing equations, a pressure-based solver with the SIMPLE scheme (Van Doormaal and Raithby, 1984) for pressure-velocity coupling was utilized. Moreover, the PRESTO! (PREssure STaggering Option) method (Patankar, 1980) was adopted as the interpolation scheme for computing cell-face pressures, which is fundamentally devised for strongly curved domains. Convergence was monitored by the common residuals as well as the computed drag coefficient on the packings and vertex value of axial velocity in a predefined point behind the packing section (at the position 0,0,125 mm). Furthermore, the overall mass balance of the system was checked for accurate conservation for all flow field results.

4. Results and discussion

4.1. Packing structures

The RBD-generated packings were characterized in terms of both global and local porosity data. The bulk porosity of all simulated structures before and after bed contraction was computed and compared with the literature data in Table 2.

The results of the bulk porosity analysis demonstrate satisfactory agreement with the empirical correlations, where the simulated void fraction values are mostly in between the range of predicted data by the published correlations. The local shrinking of pellets by 0.5% leads to some minor changes to the mean porosity values of the packing structures, of the order of 1.7% to 2.33%, (see Table 1), which is sufficiently small to not significantly affect the bed hydrodynamics.

A supplementary assessment of the packing structure was performed by benchmarking the radial void fraction distribution obtained from the simulated structures against published analytical and experimental data in Figs. 7 and 8 for packings of spheres and cylinders, respectively.

Overall, the radial porosity distribution extracted from the RBD-simulated packings for both spherical and cylindrical pellets shows a very good agreement with the empirical correlations by de Klerk (2003) and Roshani (1990). The amplitude and frequency of the oscillatory-damping pattern can be reproduced appropriately, as quantitatively evidenced by the values of the coefficient of determination, i.e. $R^2 \geq 0.8$. Remarkable is the increase of the local porosity at $(R_t - r)/d_{pv} = 2$ for packings of cylinders with N = 4.58, i.e. $N_{pv} = 4$, which evidences the presence of a hole down the tube center. Such behavior is typical for spherical packings with N around 4 (Behnam et al., 2013; Eppinger et al., 2011; Moghaddam et al., 2018; Mueller, 1993), as can be seen for the case of N = 4.1 as well (Fig. 7). It appears that a channel in the center of beds with $N_{pv} = 4$ commonly emerges, irrespective of the exact packing procedure, and is therefore a consequence of the structuring effects of the tube wall, which leads to locked configurations that prevent sliding of pellets towards the tube axis.

4.2. Mesh verification study

To investigate mesh convergence, three mesh sizes were compared for the cylinder packing with N = 2.29. Details of the mesh, including the cell size and total cell count, are given in Table 3.
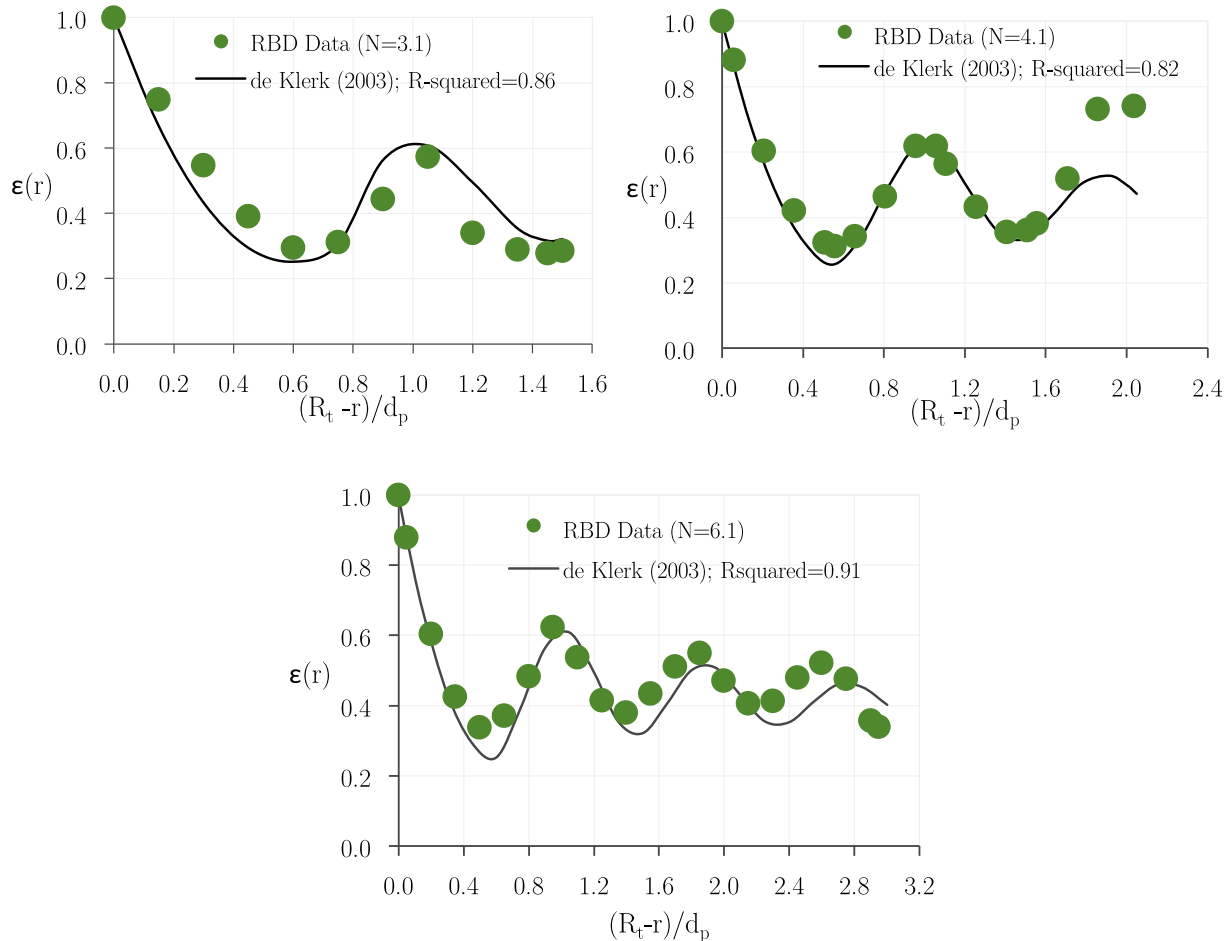

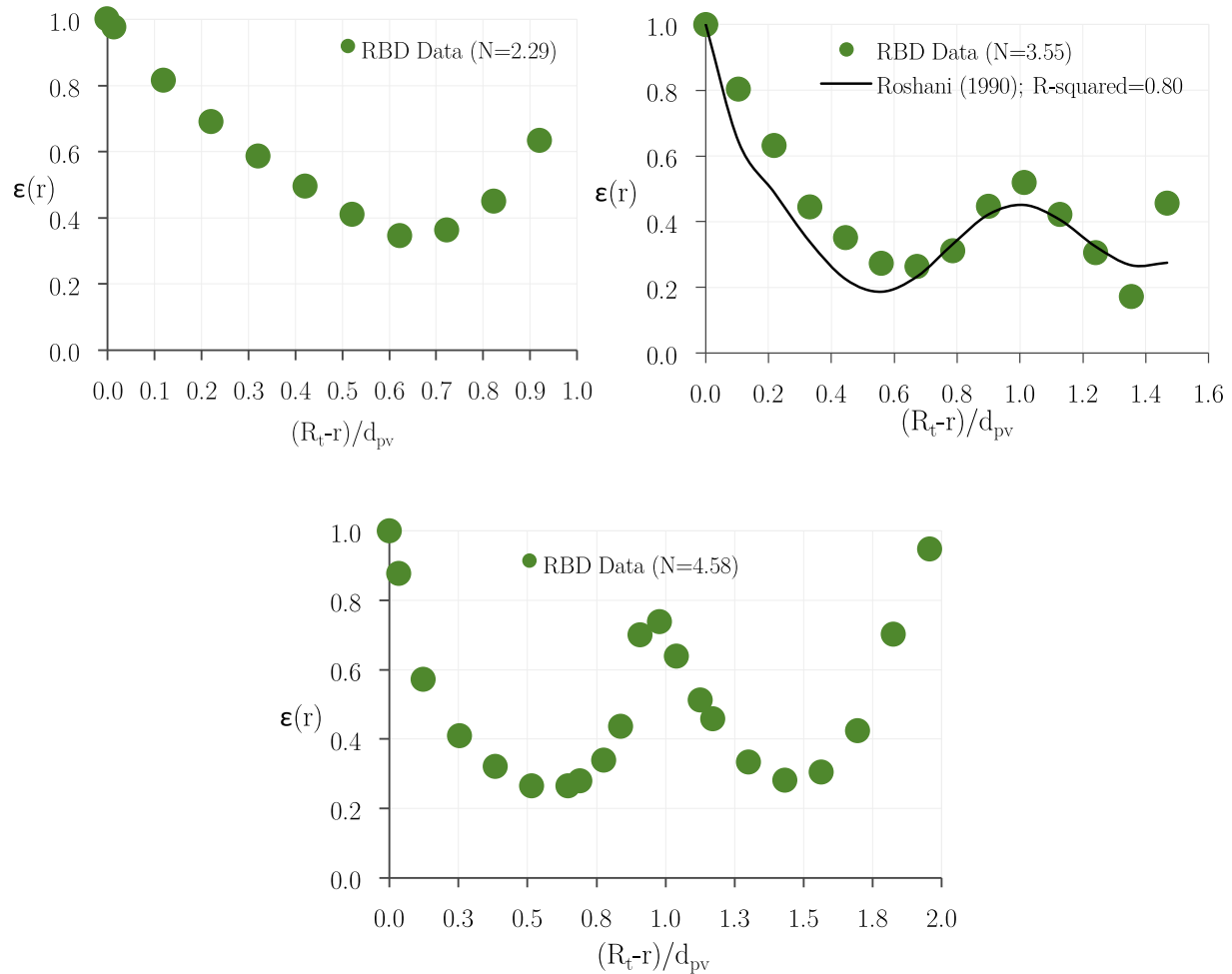**Fig. 7.** Radial void fraction profile for spherical packings.

Fig. 8. Radial void fraction profile for cylindrical packings.

Table 3
Specification of the mesh refinement study, based on the cylindrical packing with N = 2.29.

Description	Fine	Medium	Coarse
Mesh size range (mm)	0.05–0.4 (d_p/25)	0.05–0.55 (d_p/18.2)	0.05–0.8 (d_p/12.5)
Cell count ($\times 10^6$)	15.29	10.87	6.80

The three mesh levels are compared for computed axial velocity profiles along a typical line, (passing through the points (−0.011496, 0, 0.11) and (0.011496, 0, 0.11)) at bed height $z = 10d_p$ for the highest flow velocity (see Fig. 9).

The results show very good agreement between the medium and fine mesh levels over the entire length of the line. The inadequacy of the coarse mesh can be distinctly recognized, particularly at the wall regions, where the gradients are essentially steeper.

The Richardson extrapolation (RE) approach (Roache, 1998) was used to assess the discretization error of the medium mesh level for the computed velocity fields. The approach was applied based on the CFD results of pressure drop for fine and medium mesh levels to predict the value of the bed pressure drop at zero grid size, i.e. Δp_∞. Using this method, the numerical error was computed as 1.77%, which offers the medium mesh as an appropriate level for all remaining CFD simulations.

4.3. Validation study

To validate the CFD results, the computed bed pressure drops and axial velocity profiles are compared with literature data. For
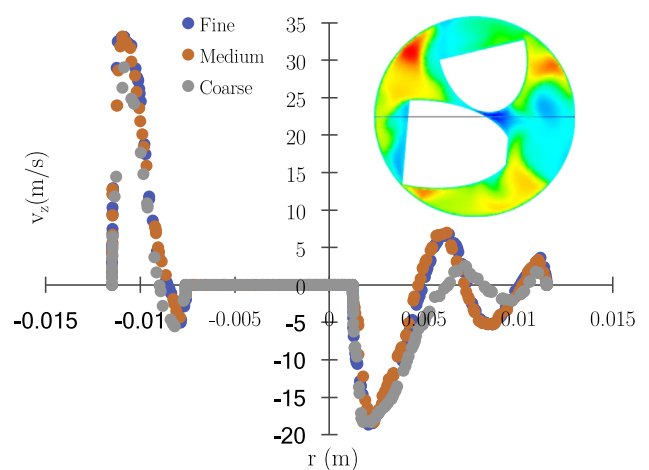

Fig. 9. Comparison between the computed axial velocity profiles obtained from three mesh levels at a typical line located at bed height $z = 10d_p$ in a cylindrical packing with N = 2.29 at $Re_p = 10000$.

the pressure drop, the correlations by Eisfeld and Schnitzlein (2001) and Cheng (2011), which properly account for the wall effects in low N-packings, are used. The former authors have performed a detailed analysis based on several thousands of experimental results to improve the correlation proposed by (Reichelt, 1972) for different types of packings. Here, a dimensionless form of the pressure drop in fixed beds, the so-called pore-based friction factor, Ψ_W, was exercised for the analysis:

$$\Psi_W = \frac{\bar{\varepsilon}^3}{1-\bar{\varepsilon}} \frac{\Delta P}{\rho u_s^2} \frac{d_{ps}}{L} \frac{1}{M} = \frac{\bar{\varepsilon} d_{ps}}{(1-\bar{\varepsilon})} \frac{\Delta P}{\rho (u_s/\bar{\varepsilon})^2 L} \frac{1}{M} = \frac{A_W}{Re_W} + B_W \quad (1)$$

where $\quad M = 1 + \dfrac{2}{3N(1-\bar{\varepsilon})} \quad$ and $\quad Re_W = \dfrac{\rho_f u_s d_{ps}}{\mu(1-\bar{\varepsilon})M} \quad (2)$

The pore-based friction factors for Eisfeld and Schnitzlein (2001) and Cheng (2011) are obtained by reformulating their original correlations in terms of Ψ_W and Re_W based on Eq. (1). The parameters and further details of the correlations are given in Table 4.

As shown in Fig. 10, the computed dimensionless pressure drops and the correlation results are in very good agreement in all flow regimes for both the spherical and cylindrical packings. The same results were also found for other packing models, which are not reported here for sake of brevity. It is noteworthy that the maximum deviation found from the correlation of (Eisfeld and Schnitzlein, 2001) is 17% for the cylindrical packing with N = 3.55 at Re_p = 5, which is reasonably justified by the range of experimental errors reported by the authors.

Table 4
Parameters of the pore-based friction factor, Eq. (1).

Author	A_W	B_W	N	Re_p
Eisfeld and Schnitzlein (2001)	154 for spheres 190 for cylinders	$[1.15N^{-2} + 0.87]^2$ for spheres $[2N_{ps}^{-2} + 0.77]^2$ for cylinders	1.6–250	0.07–17653
Cheng (2011)[*]	$\left[185 + 17\frac{\bar{\varepsilon}}{(1-\varepsilon)}\left(\frac{N}{N-1}\right)^2\right]\frac{1}{M^2}$	$\left[1.3\left(\frac{\bar{\varepsilon}}{1-\varepsilon}\right)^{1/3} + 0.03\left(\frac{N}{N-1}\right)^2\right]\frac{1}{M}$	1.1–50.5	2–5550

[*] The formula proposed by Cheng is for spheres.
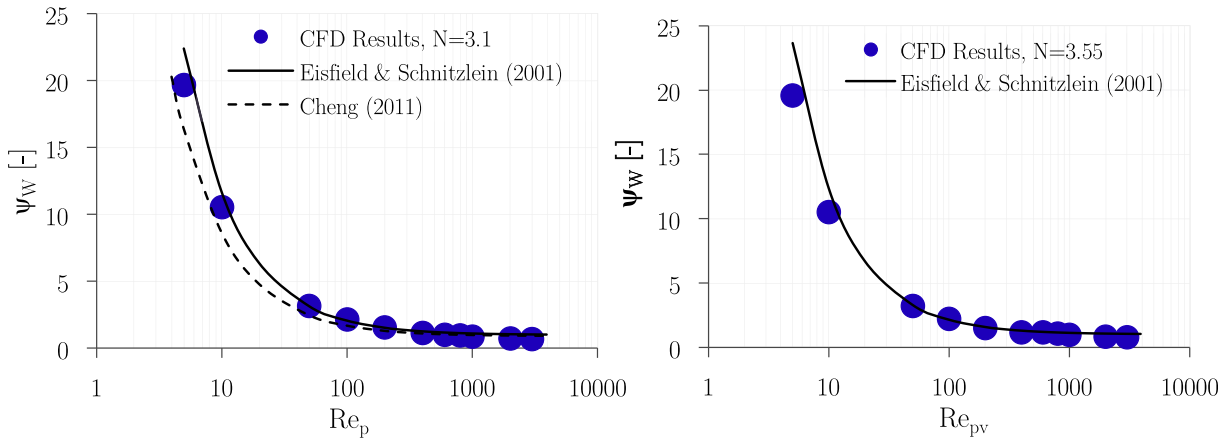
Fig. 10. Comparison between the pressure drops obtained from the CFD results and empirical correlations for packings of spheres (left) and cylinders (right).
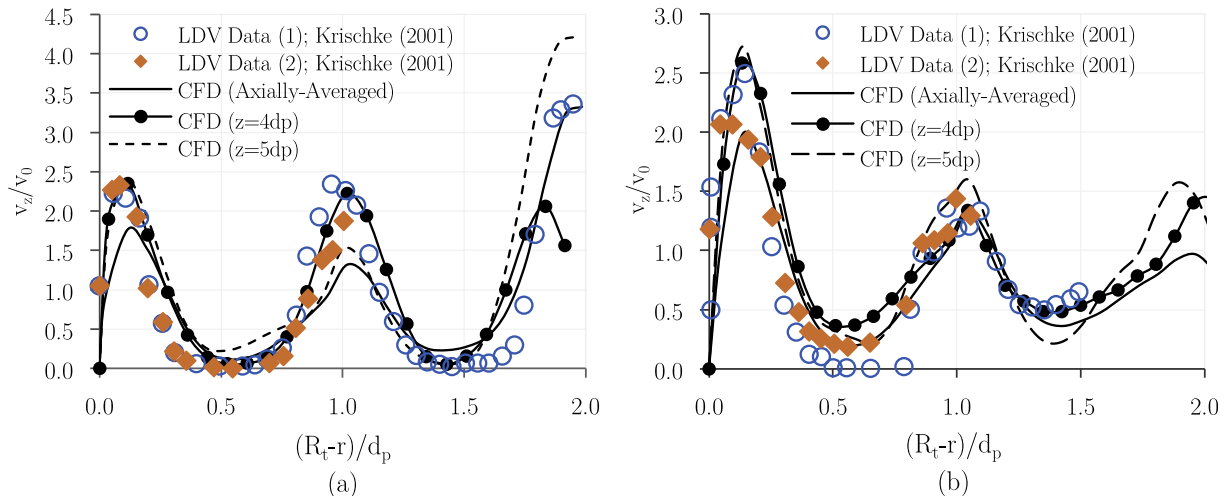
Fig. 11. Comparison between the simulated azimuthally-averaged axial velocity profiles and the experimental (LDV) data from (Krischke, 2001) at Re_p = 50; (a) N = 4.1, (b) N = 6.1.

The validity of local flow distribution was also investigated based on the experimental data from Krischke (2001). Krischke (2001) has conducted LDV measurements to probe the axial velocity distribution inside random packings of glass spheres with N = 4 and 6.15 at $Re_p = 50$.

In Fig. 11, the empirical (LDV) data of the azimuthally-averaged axial velocity profiles, extracted from two crosscuts of the setups utilized in the work of Krischke (2001), have been compared with the CFD results of azimuthally-averaged axial velocity profiles, obtained from two vertical plains at the bed heights of $4d_p$ and $5d_p$, as well as the 2D axially (bed volume)-averaged z-velocity profiles at $Re_p = 50$. Overall, the results are in reasonable agreement with the experimental data, as the typical oscillatory behavior of the radially varying axial velocity profiles are appropriately predicted both near the wall and in the inner bed regions. It is

worth mentioning that for N = 4 both CFD results and LDV data indicate the presence of a channel in the bed center, as the velocity increases significantly in this region.

4.4. 3D structure of flow fields: The validity of azimuthal averaging

Having a detailed knowledge of the flow distribution inside fixed bed reactors is crucial for the design because it strongly influences local propagation of transport scalars and thus the reactor performance. Fig. 12 exhibits two examples of the 3D structure of flow fields, in the form of contour plots of the axial velocity normalized by the inlet velocity for several cross sections, together with flow streamlines colored by the local axial velocity, for typical packings of spheres and cylinders at $Re_p = 100$.
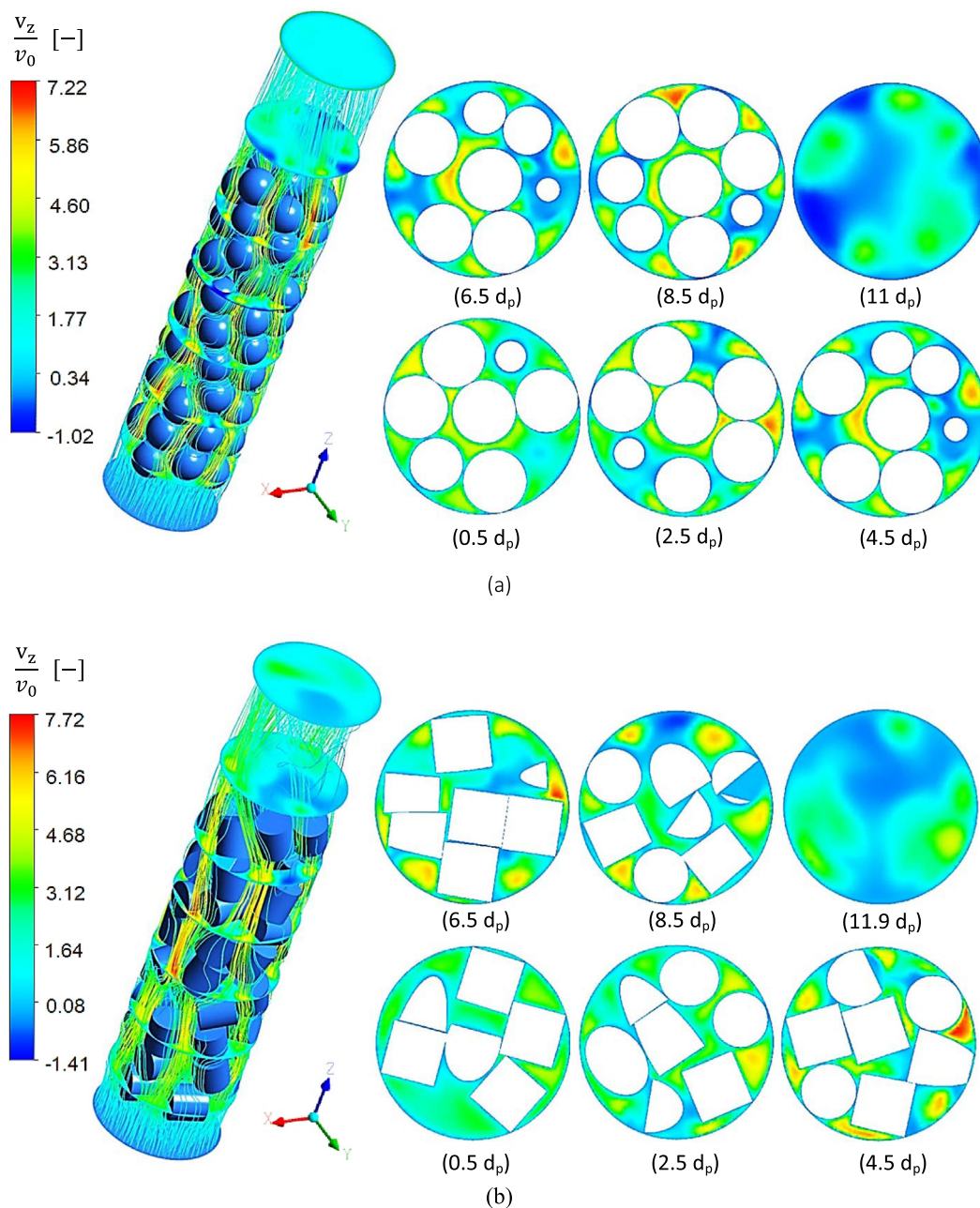
Fig. 12. Examples of 3D flow fields using streamlines and contour plots of normalized axial velocity at different cross sections at axial positions $0.5d_p$, $2.5d_p$, $4.5d_p$, $6.5d_p$, $8.5d_p$ and $+0.5d_p$ behind the packing section, for packings of spheres and cylinders with $N_{pv} = 3.1$ at $Re_p = 100$.

The contour plots of normalized axial velocities at different bed cross sections demonstrate a tremendous inhomogeneity in the velocity distribution along the packing depth, which directly arises from the structural features of the randomly-packed fixed bed arrangements. This inhomogeneity can be much more pronounced in cylindrical packings, where the sharp edges of the cylinders at each crosscut impose stronger curvatures of the streamlines along the packing. Furthermore, the contours reveal a local increase of axial velocity up to factors of 7.22 and 7.72 for packings of spheres and cylinders, respectively, for $N_{pv} = 3.1$ and $Re_p = 100$. The high velocity "hotspots" are found predominantly near the wall region and also partially in the inner regions of the packing structures. The latter phenomenon can be more easily observed in the contours of axial velocity at the central plane (XZ plane) of the packings, as shown in Fig. 13.
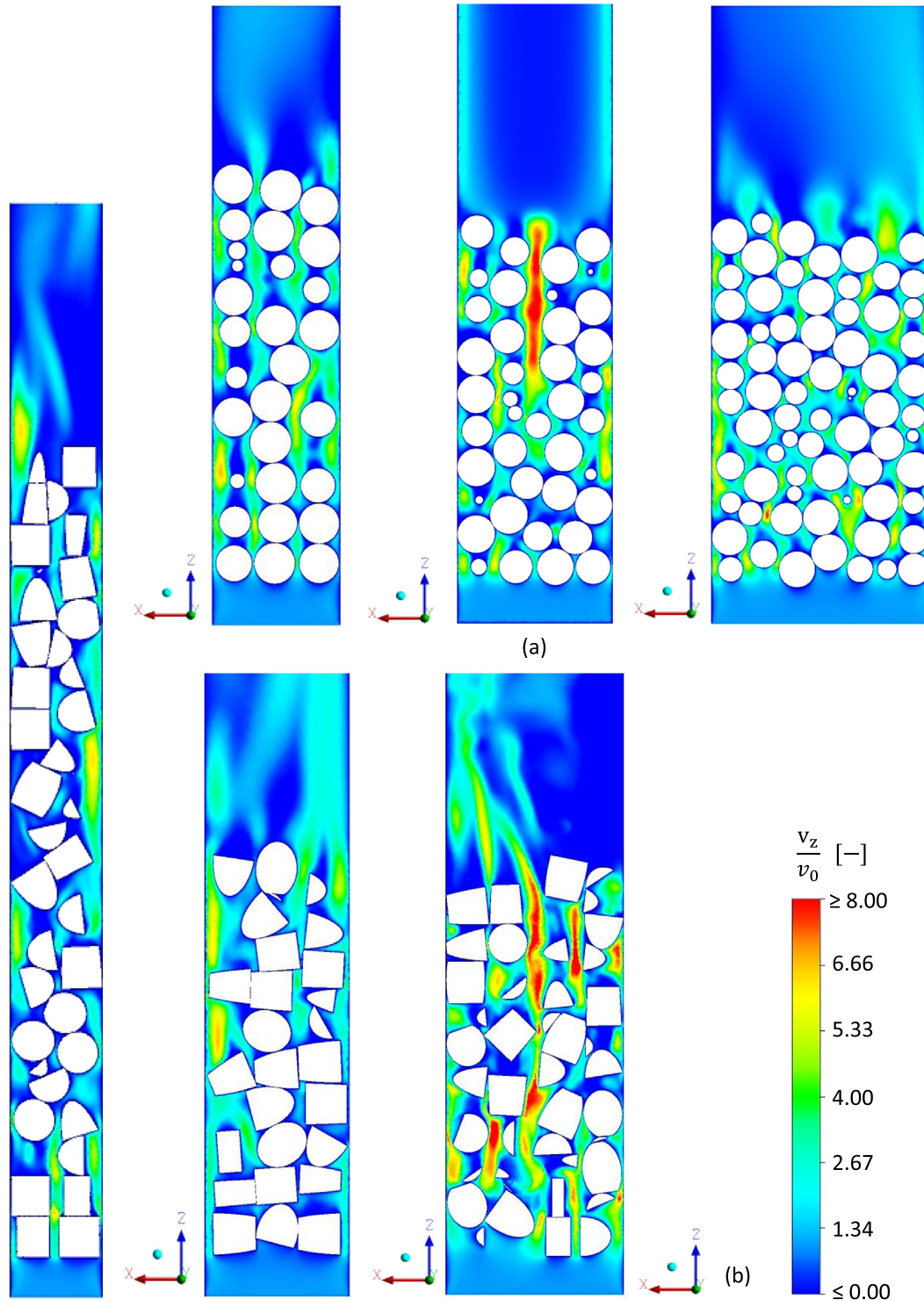
Fig. 13. Contour plots of normalized axial velocity at the central plane (XZ) of different random packings at $Re_p = 100$; (a) spheres with N = 3.1, 4.1 and 6.1; (b) cylinders with N = 2.29, 3.55 and 4.58.

As shown in the contour plots, a local increase in axial velocity mostly occurs in areas where the structure is not so dense, such as the near-wall region (the so-called wall channeling phenomenon) and connected axial interstices. However, as shown in Fig. 13, for some packings, i.e. spheres with N = 4.1 and cylinders with N = 4.58, the maximum axial velocities occur at the center of the packing, which originates from the local high porosity near the tube center in such packing structures. Such flow characteristics can be anticipated from the radial porosity profiles of these packings (see Figs. 7 and 8). Several researchers have reported similar observations, albeit only for packing of spheres with N around 4, e.g. (Behnam et al., 2013; Eppinger et al., 2011). Our CFD results demonstrate that maximum axial velocities also appear in the center of cylindrical packings with N_{pv} = 4 (see Fig. 13b). Moreover, the contour plots reveal that areas with stagnant and backflow velocity fields, i.e. vortices, are emerging in the wakes of pellets and behind the packing sections. As shown in Fig. 14, such regions become increasingly common with increasing Re_p, implicating the significant role of eddy transport at higher flow conditions in fixed bed systems. Furthermore, a quantitative analysis of such regions can provide a deeper insight into the residence time distribution (RTD) and the influence of pellet design changes on the RTD in fixed bed reactors, which is the subject of our forthcoming studies.

Fig. 15 shows the azimuthally-averaged axial velocity distributions, extracted from two different bed heights, and the axially-and-azimuthally-averaged profile, for all packing models at Re_p = 1000. The plots show the occurrence of the first maxima adjacent to the tube wall, which varies between 1.5 and 3 times the inlet superficial velocity. Furthermore, the position of the first minimum occurs approximately at $0.5d_p$ from the tube wall in packings of spheres, while this position shifts to around $0.65d_{pv}$ from the tube wall for cylindrical packings, both corresponding to the minimum in local porosity profiles shown in Fig. 8. This implies a milder radial velocity profile in fixed beds of cylinders with similar N_{pv}, which may result in a milder trend of radial dispersion of transport scalars compared to spherical packings. Nonetheless, a distinct difference between the local (azimuthally-averaged) and the global (axially-and-azimuthally-averaged) v_z/v_0 profiles can be found, specifically at the points where the local porosity has its extreme values. For example, Fig. 15(e) shows that the local azimuthally-averaged z-velocity at $z = 3.5d_p$, i.e. $v_z(r, z = 3.5d_p)$, deviates up to 76% of v_0 (with an average deviation of 18%) from the global (axially-and-azimuthally averaged) velocity $v_z(r)$ for a packing of spheres with N = 6.1 at Re_p = 1000. Similarly, Fig. 15(f) shows deviations of up to 95% (with an average deviation of 27%) for packings of cylinders with N = 2.29 at Re_p = 1000.

These local deviations culminate in narrower packing structures, e.g. N_{pv} = 2 and 3.1, where the azimuthal symmetry basically cannot be fulfilled, resulting in large heterogeneity in the radial velocity profiles along the bed axis. Moreover, considerable differences between the local and global values of v_z/v_0 can be observed in the vicinity of the tube wall in all packings. These observations
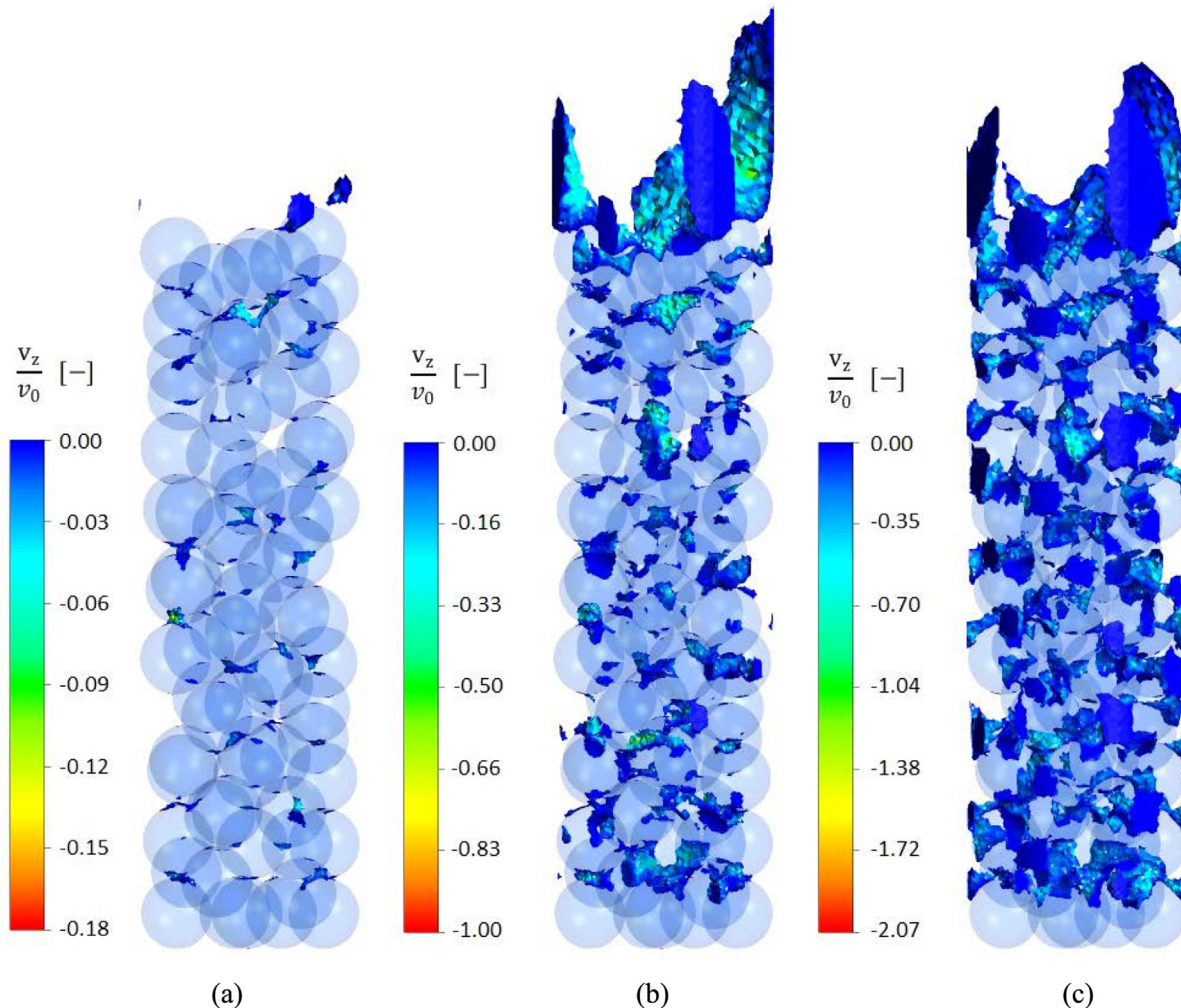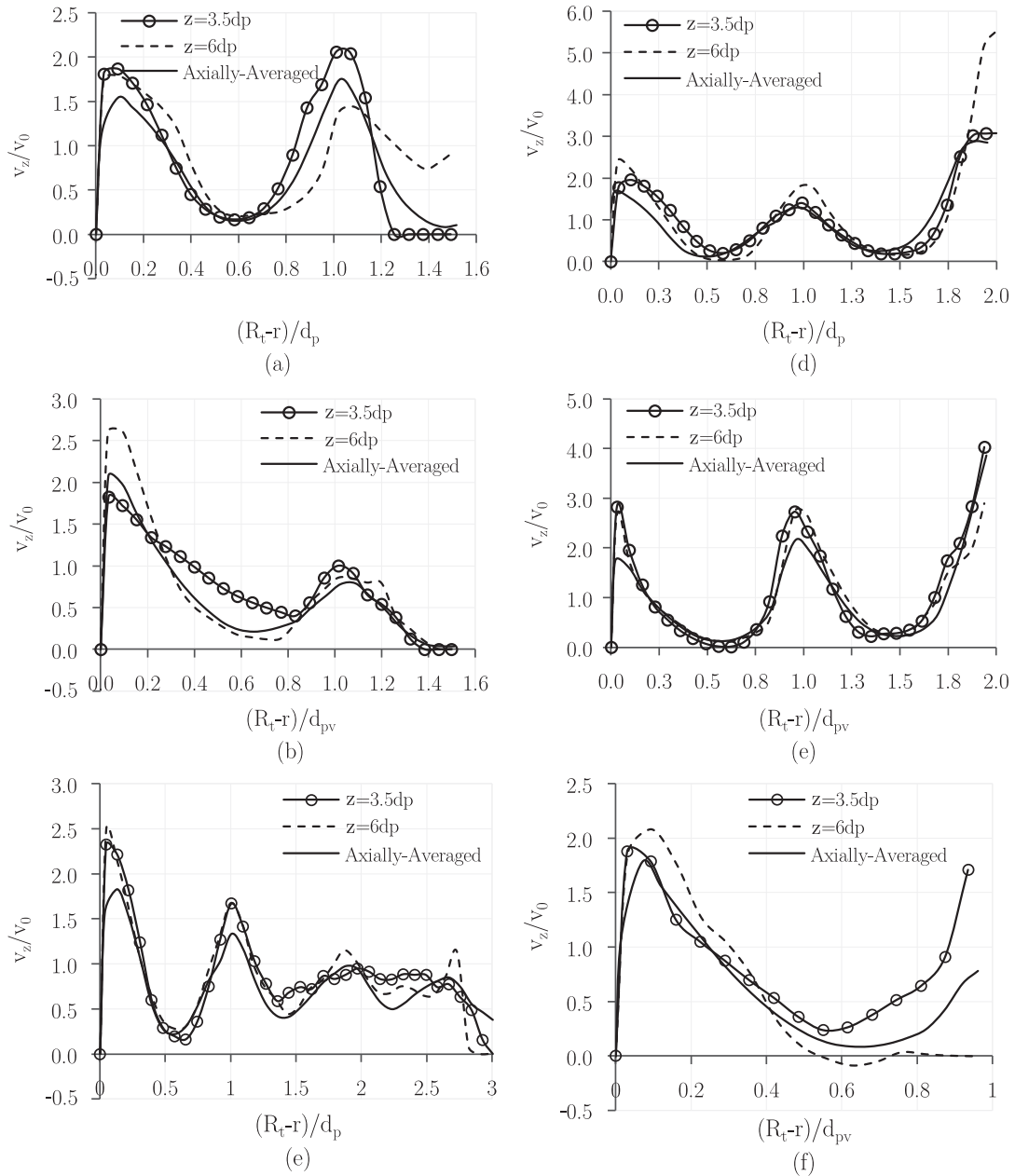

Fig. 14. Regions with stagnant and backflow velocity fields in a random packing of spheres with N = 3.1; (a) Re_p = 10, (b) Re_p = 100 and (c) Re_p = 1000.
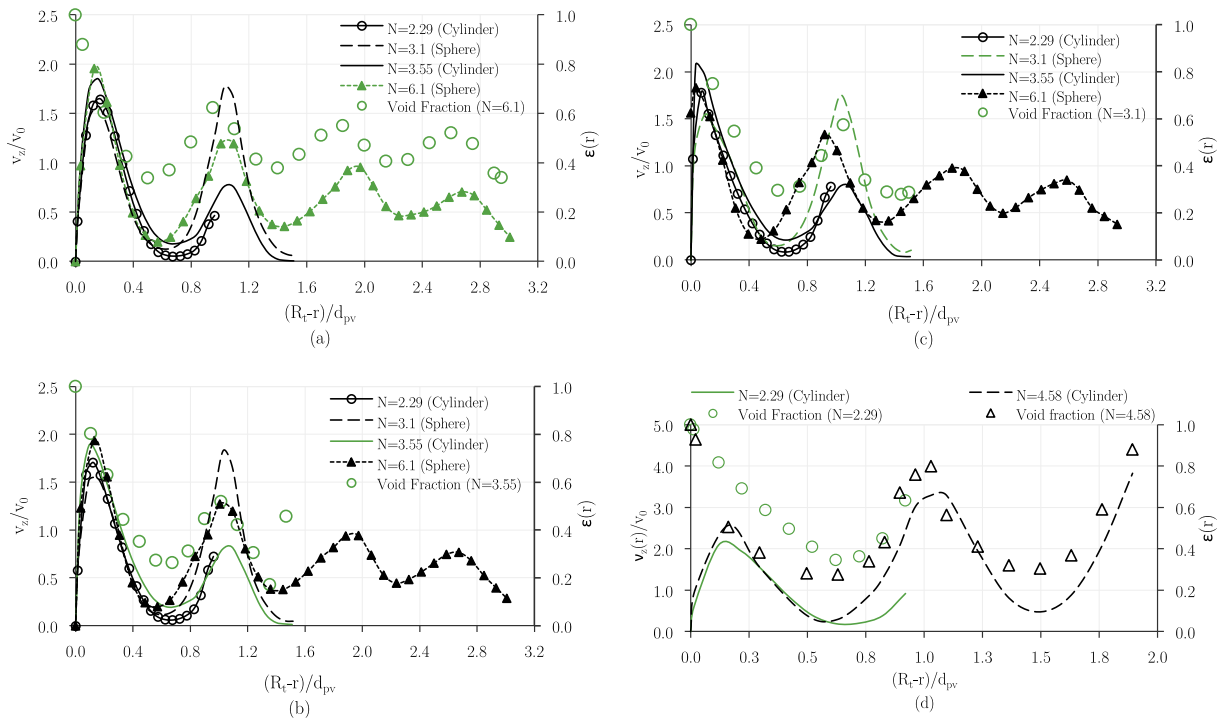
Fig. 15. Azimuthally–averaged axial velocity profiles at the cross sections z = 3.5d_p, 6d_p and axially-averaged profile at Re_p = 1000 for packings of (a) spheres with N = 3.1, (b) cylinders with N_{pv} = $_b$3.1, (c) spheres with N = 4.1, (d) cylinders with N_{pv} = 4, (e) spheres with N = 6.1, and (f) cylinders with N_{pv} = 2.

are very important, because of the crucial role of convective mechanisms in the wall-to-bed heat transfer. In the literature, global axially-and-azimuthally-averaged v_z/v_0 profiles, which can also be predicted from a modified version of the Navier-Stokes equations, e.g. (Bey and Eigenberger, 1997; Giese et al., 1998; Winterberg and Tsotsas, 2000a,b), are regularly used to improve pseudo-continuum heat transfer models. Our results suggest that using such global v_z/v_0 profiles can lead to erroneous predictions of transport properties in this region, specifically for low-N fixed bed reactors.
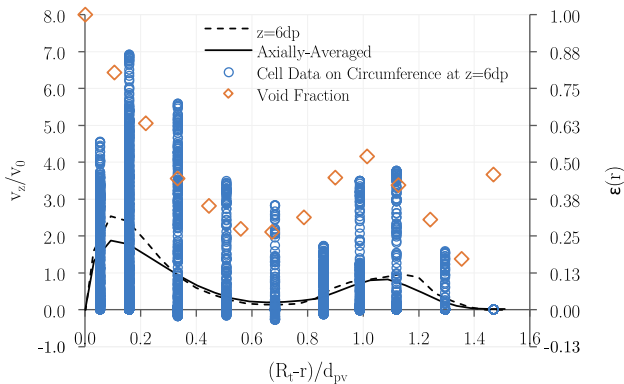
In Fig. 16, the axial-and-azimuthally-averaged axial velocity profiles at three different Re_p of 10, 100 and 1000 are plotted together with the radial porosity distribution against dimensionless distance from tube wall for some of the packing structures. Furthermore, we show the artificial axial velocity profile proposed

by Bey and Eigenberger (2001, 1997) for two cylindrical packings at Re_p = 100 (Fig. 16d).

Overall, the results demonstrate a meaningful harmony between the axially-and-azimuthally averaged bed topology data, i.e. radial porosity distribution, and axially-and-azimuthally averaged axial velocity profile in all cases, in the sense that the oscillatory pattern in the radial porosity distribution is closely reflected by the radial-dependent axial velocity profile. This harmony can be appreciated by comparing the profiles and data points with green color for a specific packing in all graphs illustrated in Fig. 16. Moreover, the normalized artificial z-velocity profiles (Fig. 16d) show peaks in the velocity ratio between 2 and 3 near the wall region, which is in agreement with the measurements of Vortmeyer and coworkers (Giese et al., 1998; Bey and Eigenberger, 1997). Nonetheless, the above averaged axial

Fig. 16. 2D (axial-and-azimuthally-averaged) axial velocity distribution together with the radial void fraction profiles; (a) $Re_p = 10$, (b) $Re_p = 100$, (c) $Re_p = 1000$, and (d) artificial z-velocity profile at $Re_p = 100$.

Fig. 17. (Axially-and-)azimuthally–averaged axial velocity profiles together with the radial porosity profile and the local axial velocity data extracted from different circumferences at the cross sections $z = 6d_p$ for cylindrical packings with $N_{pv} = 3.1$ at $Re_p = 100$.

velocities are basically positive for every Re_p, which implies the inadequacy of such flow information in reflecting the appearance of vortex regions, i.e. backflow as well as stagnant flow fields. This is also exemplified by the fact that there is a noticeable deviation (more than 400%) between the azimuthally-averaged values of axial velocities, even when obtained from a specific bed cross section and the local normalized axial velocity values. To elucidate this remarkable deviation, the local axial velocity data extracted from different circumferences at $z = 6d_p$ in packed column of cylinders with $N_{pv} = 3.1$ are compared to the (axially-and-)azimuthally-averaged axial velocity profiles at $Re_p = 100$ in Fig. 17.

The results demonstrate that the maximum relative deviation of axially-and-azimuthally-averaged velocities from the local axial velocity data occurs at the position of the first minimum in the radial porosity profile. It is worth noting that a local increase of v_z up to around $14v_0$ with respect to the azimuthally-averaged

axial velocity profile can be found at the position of the first minimum in the radial porosity profile. This result highlights to what extent the averaging of velocity fields (or the exertion of artificial velocity profiles based on averaged porosity data) in modeling fixed beds neglects the localized phenomena at the pellet scale, which can lead to erroneous predictions of the behavior of transport scalars inside the reactors.

5. Conclusions

A robust and efficient workflow was introduced to simulate the hydrodynamics in fixed beds containing non-spherical pellets. The workflow, entitled the RBD-CFD approach, consists of three main sequences, starting with physical simulation of random packings using the RBD-based packing algorithm proposed by the present authors (Moghaddam et al., 2018), followed by a contact point treatment in the computer-generated structures, and creation of an inflationary volume mesh topology using an ad hoc python-based script in ANSYS Workbench 16.2. The methodology was implemented and validated for a discrete-pellet CFD study (using ANSYS Fluent 16.2) of the velocity field and pressure drop in both spherical and cylindrical packing structures with tube-to-pellet diameter ratio N ranging from 2.29 to 6.1.

The fidelity and robustness of the RBD algorithm to generate appropriate packing structures of non-spherical pellets were discussed and evidenced. The distinct advantages, over more conventional glued-sphere DEM approaches, are a better representation of the sharp edges of the particles and avoidance of any particle overlap. Furthermore, the algorithm benefits from a more rigorous approach to handle resting contact phenomenon compared to Blender software, as discussed in our previous contribution [1], which is a substantial improvement in the configuration generation of a resolved-particle CFD model of fixed bed systems. The inflationary meshing scheme has been applied to random packing structures using a combination of patch confirming and patch

independent approaches. This approach does not only provide a fine mesh to appropriately capture details of the phenomena occurring at the contact regions, but it also facilitates the solution convergence in the turbulent flow regime without any need for manipulating the under-relaxation factors, which is a routine method contrived by most other researchers to resolve the convergence problem in such complicated flow domains.

The CFD results of the flow hydrodynamics were validated by comparing the pressure drop as well as azimuthally-averaged axial velocity profiles to published empirical data. The 3D flow field results reveal a remarkable influence of local structure on the velocity distribution at the pellet scale, where the presence of wall effects, i.e. flow channeling, across the entire tube radius can be clearly elucidated by contour plots of the velocity field in such narrow tubular fixed beds. It is also demonstrated that azimuthal-averaging of the 3D velocity field along the bed, which has been an advancement in plug flow idealization in classical modelling, cannot reflect the vortex regions (areas with negative axial velocities) inside the structure, leading to an error in the local velocity values by up to 400% of the inlet superficial velocity. This deviation can even culminate in narrower structures, where the spatial heterogeneities are maximized along the central bed axis. This explains the inadequacy of even modified versions of pseudo-continuum approaches in predicting the local transport scalars inside such fixed bed reactors. This contribution, with the aid of validated data, offers the RBD-CFD method as a robust design philosophy within the context of "Numerical Experiments", which enables a proper understanding of complex physio-chemical phenomena at the pellet scale of non-spherical fixed beds.

Conflict of interest

None declared.

References

Augier, F., Idoux, F., Delenne, J.Y., 2010. Numerical simulations of transfer and transport properties inside packed beds of spherical particles. Chem. Eng. Sci. 65, 1055–1064. https://doi.org/10.1016/j.ces.2009.09.059.

Baker, M.J., Young, P.G., Tabor, G.R., 2011. Image based meshing of packed beds of cylinders at low aspect ratios using 3d MRI coupled with computational fluid dynamics. Comput. Chem. Eng. 35, 1969–1977. https://doi.org/10.1016/j.compchemeng.2011.03.017.

Beguin, R., Philippe, P., Faure, Y.-H., 2013. Pore-scale flow measurements at the interface between a sandy layer and a model porous medium: application to statistical modeling of contact erosion. J. Hydraul. Eng. 139, 1–11. https://doi.org/10.1061/(ASCE)HY.1943-7900.0000641.

Behnam, M., Dixon, A.G., Nijemeisland, M., Stitt, E.H., 2013. A new approach to fixed bed radial heat transfer modeling using velocity fields from computational fluid dynamics simulations. Ind. Eng. Chem. Res. 52, 15244–15261. https://doi.org/10.1021/ie4000568.

Bey, O., Eigenberger, G., 2001. Gas flow and heat transfer through catalyst filled tubes. Int. J. Therm. Sci. 40, 152–164. https://doi.org/10.1016/S1290-0729(00)01204-7.

Bey, O., Eigenberger, G., 1997. Fluid flow through catalyst filled tubes 52.

Boccardo, G., Augier, F., Haroun, Y., Ferre, D., Marchisio, D.L., 2015. Validation of a novel open-source work-flow for the simulation of packed-bed reactors. Chem. Eng. J. 279, 809–820. https://doi.org/10.1016/j.cej.2015.05.032.

Calis, H.P.A., Nijenhuis, J., Paikert, B.C., Dautzenberg, F.M., Van Den Bleek, C.M., 2001. CFD modeling and experimental validation of pressure drop and flow profile in a novel structured catalytic reactor packing. Chem. Eng. Sci. 56, 1713–1720. https://doi.org/10.1016/S0009-2509(00)00400-0.

Cheng, N., 2011. Wall effect on pressure drop in packed beds. Powder Technol. 210, 261–266. https://doi.org/10.1016/j.powtec.2011.03.026.

Coussirat, M., Guardo, A., Mateos, B., Egusquiza, E., 2007. Performance of stress-transport models in the prediction of particle-to-fluid heat transfer in packed beds. Chem. Eng. Sci. 62, 6897–6907. https://doi.org/10.1016/j.ces.2007.08.071.

De Klerk, A., 2003. Voidage variation in packed beds at small column to particle diameter ratio. AIChE J. 49, 2022–2029. https://doi.org/10.1002/aic.690490812.

Dijksman, J.A., Rietz, F., Lorincz, K.A., Van Hecke, M., Losert, W., 2012. Invited article: Refractive index matched scanning of dense granular materials. Rev. Sci. Instrum. 83. https://doi.org/10.1063/1.3674173.

Dixon, A.G., 1988. Correlations for wall and particle shape effects on fixed bed bulk voidage. Can. J. Chem. Eng. 66, 705–708. https://doi.org/10.1002/cjce.5450660501.

Dixon, A.G., Ertan Taskin, M., Nijemeisland, M., Stitt, H.H., Taskin, M.E., Nijemeisland, M., Stitt, E.H., 2011. Systematic mesh development for 3D CFD simulation of fixed beds: Single sphere study. Comput. Chem. Eng. 35, 1171–1185. https://doi.org/10.1016/j.compchemeng.2010.12.006.

Dixon, A.G., Nijemeisland, M., 2001. CFD as a design tool for fixed-bed reactors. Ind. Eng. Chem. Res., 5246–5254 https://doi.org/10.1021/ie001035a.

Dixon, A.G., Nijemeisland, M., Stitt, E.H., 2013. Systematic mesh development for 3D CFD simulation of fixed beds: Contact points study. Comput. Chem. Eng. 48, 135–153. https://doi.org/10.1016/j.compchemeng.2012.08.011.

Dixon, A.G., Nijemeisland, M., Stitt, E.H., 2006. Packed tubular reactor modeling and catalyst design using computational fluid dynamics. Adv. Chem. Eng. 31, 307–389. https://doi.org/10.1016/S0065-2377(06)31005-8.

Dixon, A.G., Walls, G., Stanness, H., Nijemeisland, M., Stitt, E.H., 2012. Experimental validation of high Reynolds number CFD simulations of heat transfer in a pilot-scale fixed bed tube. Chem. Eng. J. 200–202, 344–356. https://doi.org/10.1016/j.cej.2012.06.065.

Dong, Y., Sosna, B., Korup, O., Rosowski, F., Horn, R., 2017. Investigation of radial heat transfer in a fixed-bed reactor: CFD simulations and profile measurements. Chem. Eng. J. 317, 204–214. https://doi.org/10.1016/j.cej.2017.02.063.

Eisfeld, B., Schnitzlein, K., 2001. The influence of confining walls on the pressure drop in packed beds. Chem. Eng. Sci. 56, 4321–4329.

Eppinger, T., Seidler, K., Kraume, M., 2011. DEM-CFD simulations of fixed bed reactors with small tube to particle diameter ratios. Chem. Eng. J. 166, 324–331. https://doi.org/10.1016/j.cej.2010.10.053.

Foumeny, E.A., Moallemi, H.A., Mcgreavy, C., Castro, J.A.A., 1991. Elucidation of mean voidage in packed beds. Can. J. Chem. Eng. https://doi.org/10.1002/cjce.5450690425.

Freiwald, M.G., Paterson, W.R., 1992. Accuracy of model predictions and reliability of experimental data for heat transfer in packed beds. Chem. Eng. Sci. 47, 1545–1560. https://doi.org/10.1016/0009-2509(92)85003-T.

Freund, H., Bauer, J., Zeiser, T., Emig, G., 2005. Detailed simulation of transport processes in fixed-beds. Ind. Eng. Chem. Res. 44, 6423–6434. https://doi.org/10.1021/ie0489453.

Freund, H., Zeiser, T., Huber, F., Klemm, E., Brenner, G., Durst, F., Emig, G., 2003. Numerical simulations of single phase reacting flows in randomly packed fixed-bed reactors and experimental validation. Chem. Eng. Sci. 58, 903–910. https://doi.org/10.1016/S0009-2509(02)00622-X.

Giese, M., Rottschafer, K., Vortmeyer, D., 1998. Measured and modeled superficial flow profiles in packed beds with liquid flow. AIChE J. 44, 484–490. https://doi.org/10.1002/aic.690440225.

Harshani, H.M.D., Galindo-Torres, S.A., Scheuermann, A., Muhlhaus, H.B., 2016. Experimental study of porous media flow using hydro-gel beads and LED based PIV. Meas. Sci. Technol. 28, 15902.

Höhner, D., Wirtz, S., Scherer, V., 2014. A study on the influence of particle shape and shape approximation on particle mechanics in a rotating drum using the discrete element method. Powder Technol. 253, 256–265. https://doi.org/10.1016/j.powtec.2013.11.023.

Jafari, a., Zamankhan, P., Mousavi, S.M., Pietarinen, K., 2008. Modeling and CFD simulation of flow behavior and dispersivity through randomly packed bed reactors. Chem. Eng. J. 144, 476–482. https://doi.org/10.1016/j.cej.2008.07.033.

Krischke, A.M., 2001. Modellierung und experimentelle Untersuchung von Transportprozessen in durchstromten Schuttungen. FORTSCHRITT BERICHTE-VDI R. 3 VERFAHRENSTECHNIK. VDI VERLAG.

Kwapinski, W., Winterberg, M., Tsotsas, E., Mewes, D., 2004. Modeling of the wall effect in packed bed adsorption. Chem. Eng. Technol. 27, 1179–1186. https://doi.org/10.1002/ceat.200407001.

Lu, G., Third, J.R., Müller, C.R., 2015. Discrete element models for non-spherical particle systems: From theoretical developments to applications. Chem. Eng. Sci. 127, 425–465. https://doi.org/10.1016/j.ces.2014.11.050.

Ma, H., Zhao, Y., 2018. CFD-DEM investigation of the fluidization of binary mixtures containing rod-like particles and spherical particles in a fluidized bed. Powder Technol. 336, 533–545. https://doi.org/10.1016/j.powtec.2018.06.034.

Magnico, P., 2003. Hydrodynamic and transport properties of packed beds in small tube-to-sphere diameter ratio: pore scale simulation using an Eulerian and a Lagrangian approach. Chem. Eng. Sci. 58, 5005–5024. https://doi.org/10.1016/S0009-2509(03)00282-3.

Mantle, M.D., Sederman, A.J., Gladden, L.F., 2001. Single-and two-phase flow in fixed-bed reactors: MRI flow visualisation and lattice-Boltzmann simulations. Chem. Eng. Sci. 56, 523–529.

Marigo, M., Stitt, E.H., 2015. Discrete element method (DEM) for industrial applications: Comments on calibration and validation for the modelling of cylindrical pellets. KONA Powder Part. J. 32, 236–252.

McGreavy, C., Foumeny, E.A., Javed, K.H., 1986. Characterization of transport properties for fixed bed in terms of local bed structure and flow distribution. Chem. Eng. Sci. 41, 787–797.

Moghaddam, E.M., Foumeny, E.A., Stankiewicz, A.I., Padding, J.T., 2018. A rigid body dynamics algorithm for modelling random packing structures of non-spherical and non-convex pellets. Ind. Eng. Chem. Res. 57, 14988–15007. https://doi.org/10.1021/acs.iecr.8b03915.

Mueller, G.E., 1993. Angular void fraction distributions in randomly packed fixed beds of uniformly sized spheres in cylindrical containers. Powder Technol. 77, 313–319. https://doi.org/10.1016/0032-5910(93)85023-3.

Nijemeisland, M., Dixon, A.G., 2004. CFD study of fluid flow and wall heat transfer in a fixed bed of spheres. AIChE J. 50, 906–921. https://doi.org/10.1002/aic.10089.

Nijemeisland, M., Dixon, A.G., 2001. Comparison of CFD simulations to experiment for convective heat transfer in a gas-solid fixed bed. Chem. Eng. J. 82, 231–246. https://doi.org/10.1016/S1385-8947(00)00360-0.

Papageorgiou, J.N., Froment, G.F., 1995. Simulation models accounting for radial voidage profiles in fixed-bed reactors. Chem. Eng. Sci. 50, 3043–3056. https://doi.org/10.1016/0009-2509(95)00138-U.

Partopour, B., Dixon, A.G., 2017. An integrated workflow for resolved-particle packed bed models with complex particle shapes. Powder Technol. 322, 258–272. https://doi.org/10.1016/j.powtec.2017.09.009.

Patankar, S., 1980. Numerical Heat Transfer and Fluid Flow. CRC Press.

Pistocchini, L., Garone, S., Motta, M., 2016. Porosity and pressure drop in packed beds of spheres between narrow parallel walls. Chem. Eng. J. 284, 802–811. https://doi.org/10.1016/j.cej.2015.08.047.

Rakotonirina, A.D., Wachs, A., 2018. Grains3D, a flexible DEM approach for particles of arbitrary convex shape - Part II: Parallel implementation and scalable performance. Powder Technol. 324, 18–35. https://doi.org/10.1016/j.powtec.2017.10.033.

Reichelt, W., 1972. Zur Berechnung des Druckverlustes einphasig durchströmter Kugel-und Zylinderschüttungen. Chemie Ing. Tech., 1068–1071 https://doi.org/10.1002/cite.330441806.

Ren, X., Stapf, S., Blümich, B., 2005. Magnetic resonance visualisation of flow and pore structure in packed beds with low ratio. Chem. Eng. Technol. 28, 219–225. https://doi.org/10.1002/ceat.200407092.

Roache, P.J., 1998. Verification of codes and calculations. AIAA J. 36, 696–702.

Robbins, D.J., El-Bachir, M.S., Gladden, L.F., Cant, R.S., von Harbou, E., 2012. CFD modeling of single-phase flow in a packed bed with MRI validation. AIChE J. 58, 3904–3915.

Romkes, S.J., Dautzenberg, F., van den Bleek, C., Calis, H.P., 2003. CFD modelling and experimental validation of particle-to-fluid mass and heat transfer in a packed bed at very low channel to particle diameter ratio. Chem. Eng. J. 96, 3–13. https://doi.org/10.1016/j.cej.2003.08.026.

Roshani, S., 1990. Elucidation of Local and Global Structural Prperties of Packed Bed Configurations. The University of Leeds.

Seelen, L.J.H., Padding, J.T., Kuipers, J.A.M., 2018. A granular discrete element method for arbitrary convex particle shapes: Method and packing generation. Chem. Eng. Sci. 189, 84–101. https://doi.org/10.1016/j.ces.2018.05.034.

Singhal, A., Cloete, S., Radl, S., Quinta-Ferreira, R., Amini, S., 2017a. Heat transfer to a gas from densely packed beds of cylindrical particles. Chem. Eng. Sci. 172, 1–12. https://doi.org/10.1016/j.ces.2017.06.003.

Singhal, A., Cloete, S., Radl, S., Quinta-Ferreira, R., Amini, S., 2017b. Heat transfer to a gas from densely packed beds of monodisperse spherical particles. Chem. Eng. J. 314, 27–37. https://doi.org/10.1016/j.cej.2016.12.124.

Suekane, T., Yokouchi, Y., Hirai, S., 2003. Inertial flow structures in a simple-packed bed of spheres. AIChE J. 49, 10–17.

Taskin, M.E., Dixon, A.G., Nijemeisland, M., Stitt, E.H., 2008. CFD study of the influence of catalyst particle design on steam reforming reaction heat effects in narrow packed tubes. Ind. Chem. Res. 47, 5966–5975. 0.1021/ie800315d.

Van Doormaal, J.P., Raithby, G.D., 1984. Enhancements of the SIMPLE method for predicting incompressible fluid flows. Numer. heat Transf. 7, 147–163.

Vortmeyer, D., Haidegger, E., 1991. Discrimination of three approaches to evaluate heat fluxes for wall-cooled fixed bed chemical reactors. Chem. Eng. Sci. 46, 2651–2660. https://doi.org/10.1016/0009-2509(91)80058-7.

Wachs, A., Girolami, L., Vinay, G., Ferrer, G., 2012. Grains3D, a flexible DEM approach for particles of arbitrary convex shape — Part I: Numerical model and validations. Powder Technol. 224, 374–389. https://doi.org/10.1016/j.powtec.2012.03.023.

Wehinger, G.D., Eppinger, T., Kraume, M., 2015a. Evaluating catalytic fixed-bed reactors for dry reforming of methane with detailed CFD. Chemie-Ingenieur-Technik 87. https://doi.org/10.1002/cite.201400153.

Wehinger, G.D., Eppinger, T., Kraume, M., 2015b. Detailed numerical simulations of catalytic fixed-bed reactors: Heterogeneous dry reforming of methane. Chem. Eng. Sci. 122, 197–209. https://doi.org/10.1016/j.ces.2014.09.007.

Wehinger, G.D., Fu, C., Kraume, M., 2017a. Contact modifications for CFD simulations of fixed-bed reactors. Cylindrical Particles. https://doi.org/10.1021/acs.iecr.6b03596.

Wehinger, G.D., Füterer, C., Kraume, M., 2017b. Contact modifications for CFD simulations of fixed-bed reactors: Cylindrical particles. Ind. Eng. Chem. Res. 56, 87–99. https://doi.org/10.1021/acs.iecr.6b03596.

Winterberg, M., Tsotsas, E., 2000a. Modelling of heat transport in beds packed with spherical particles for various bed geometries and/or thermal boundary conditions. Int. J. Therm. Sci. 39, 556–570. https://doi.org/10.1016/S1290-0729(00)00251-9.

Winterberg, M., Tsotsas, E., 2000b. Impact of tube-to-particle-diameter ratio on pressure drop in packed beds. AIChE J. 46, 1084–1088. https://doi.org/10.1002/aic.690460519.

Winterberg, M., Tsotsas, E., Krischke, A., Vortmeyer, D., 2000. A simple and coherent set of coefficients for modelling of heat and mass transport with and without chemical reaction in tubes filled with spheres. Chem. Eng. Sci. 55, 967–979. https://doi.org/10.1016/S0009-2509(99)00379-6.

Wu, Y., An, X., Yu, A.B., 2017. DEM simulation of cubical particle packing under mechanical vibration. Powder Technol. 314, 89–101. https://doi.org/10.1016/j.powtec.2016.09.029.

Yan, Z., Wilkinson, S.K., Stitt, E.H., Marigo, M., 2015. Discrete element modelling (DEM) input parameters: understanding their impact on model predictions using statistical analysis. Comput. Part. Mech. 2, 283–299.

Yang, J., Wu, J., Zhou, L., Wang, Q., 2016. Computational study of fluid flow and heat transfer in composite packed beds of spheres with low tube to particle diameter ratio. Nucl. Eng. Des. 300, 85–96. https://doi.org/10.1016/j.nucengdes.2015.10.030.

Zhong, W., Yu, A., Liu, X., Tong, Z., Zhang, H., 2016. DEM/CFD-DEM modelling of non-spherical particulate systems: theoretical developments and applications. Powder Technol. 302, 108–152. https://doi.org/10.1016/j.powtec.2016.07.010.